Cell-substrate impedance fluctuations of single amoeboid cells encode cell-shape and adhesion dynamics

Helmar Leonhardt,[1] Matthias Gerhardt,[1] Nadine Höppner,[2] Kirsten Krüger,[1] Marco Tarantola,[2] and Carsten Beta[1,2,*]

[1]*Institute of Physics and Astronomy, University of Potsdam, Karl-Liebknecht Strasse 24/25, 14476 Potsdam, Germany*

[2]*Max Planck Institute for Dynamics and Self-Organization, Am Fassberg 17, 37077 Göttingen, Germany*

(Received 27 July 2015; revised manuscript received 8 December 2015; published 25 January 2016)

We show systematic electrical impedance measurements of single motile cells on microelectrodes. Wild-type cells and mutant strains were studied that differ in their cell-substrate adhesion strength. We recorded the projected cell area by time-lapse microscopy and observed irregular oscillations of the cell shape. These oscillations were correlated with long-term variations in the impedance signal. Superposed to these long-term trends, we observed fluctuations in the impedance signal. Their magnitude clearly correlated with the adhesion strength, suggesting that strongly adherent cells display more dynamic cell-substrate interactions.

DOI: 10.1103/PhysRevE.93.012414

I. INTRODUCTION

Adhesion and motility of adherent eukaryotic cells is central to many biological phenomena ranging from morphogenesis and wound healing to cancer metastasis. It relies on cell-substrate interactions that are mediated through a large network of dynamically interacting molecules [1]. For example, in many motile cells, focal complexes and focal adhesions link the actin cortex via integrins to the substratum [2,3]. Understanding the dynamics of adhesion sites and its dependence on signaling events, mechanical cues, and structural factors is a major focus of current motility research (see, e.g., Refs. [4,5]).

The social amoeba *Dictyostelium discoideum* has evolved into a popular model to study eukaryotic cell motility and adhesion. Viewed under a bright-field microscope, the motility of surface-attached *Dictyostelium* cells involves cyclic shape changes of membrane protrusion and retraction, resulting in irregular oscillations of the projected cell area [6]. In *Dictyostelium*, no integrin-mediated focal adhesions are present. Instead, several other proteins related to cell-substrate adhesion were identified, including the actin anchoring protein talin [7], the nine-transmembrane proteins Phg1 [8] and SadA [9], the disintegrin domain protein AmpA [10], and the type I transmembrane protein SibA [11]. Also innate nonspecific adhesion via cell surface glycoproteins has been suggested to play an important role for *Dictyostelium* cell-substrate adhesion [12,13].

On the subcellular scale, adhesion regions establish cell-substrate contacts and are visible under a reflection interference contrast microscope [6]. By the same technique, actin foci—dense localized regions of increased F-actin concentration in the cell cortex—have been discovered and associated with cell-substrate adhesion in *Dictyostelium* [14]. In particular, traction force microscopy measurements suggested that traction forces are transmitted through these foci [14,15]. They also reveal the spatial distribution of traction forces exerted by *D. discoideum* cells during their movement cycle on elastic substrata [16,17], demonstrating that traction stress patterns in the front and back of the cell correspond to the adhesion regions observed in Refs. [6,15].

Today, a variety of noninvasive methods are applied to study cell-substrate interactions *in vivo* (for a review see Ref. [18]). Besides optical methods, also electrical techniques have been employed to investigate cell-substrate interactions and play an important role in current biosensor concepts [19]. Using electric fields to sense and monitor the activity of cultured cells on microelectrodes is known as electric cell-substrate impedance sensing (ECIS) [20,21], a common technique to perform population measurements of different processes, such as cell adhesion [22], viability [23], protrusion formation [24], and chemotaxis [25]. Recently, ECIS recordings were used to characterize collective synchronized oscillations of cell-substrate contacts during aggregation of starved *D. discoideum* amoebae [26]. Optical and acoustic methods were utilized to relate synchronous changes in cell density, morphology, and cell-substrate distance to the measured time evolution of the impedance [27].

In contrast to previous ECIS measurements on cell populations, we present in this article cell-substrate impedance measurements of single *D. discoideum* cells on microelectrodes. Cell-shape changes were captured by time-lapse microscopy, allowing us to relate such events to changes in the kinetics of the impedance. For our analysis we collected more than a hundred impedance time series of vegetative wild-type cells and four mutant strains with altered cell-substrate adhesiveness (*tal*A$^-$, *nap*A$^-$, *amp*A$^-$, and *GFP-α-tubulin*). The magnitude of impedance fluctuations differs for the adhesion-deficient mutants and is correlated with the order of increasing adhesion strengths of these cell lines that we determined independently in a shear stress detachment assay and by atomic force microscopy measurements.

II. MATERIALS AND METHODS

A. Experimental setup

For measuring the cell-substrate impedance a custom-made cell-substrate impedance sensor (CSIS) was developed using commercially available electronic parts including data aquisition (DAQ) hardware (NI PCI-6120 board, National Instruments, München, Germany) and a data processing platform

*Corresponding author: beta@uni-potsdam.de

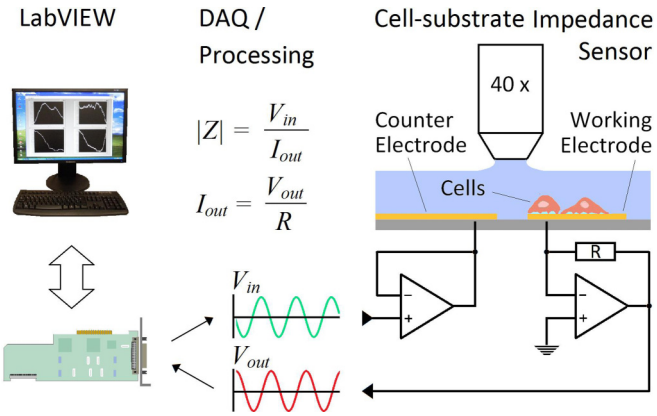

FIG. 1. Experimental setup. A voltage signal, controlled by LABVIEW software, is applied to the counter electrode of the cell-substrate impedance sensor and the current measured at the working electrode by a current-to-voltage converter. The impedance is given by $Z = V_{\text{in}}/I_{\text{out}}$.

(LABVIEW, National Instruments, München, Germany); see Fig. 1. The key part of the device is a microelectrode array interfacing the cells to the DAQ hardware. For single-cell recordings microelectrode arrays (MEAs) from Multi Channel Systems (Reutlingen, Germany) were used, with 59 50-μm TiN square electrodes, and ECIS cultureware 8W1E DD PET (Applied Biophysics Inc., Troy, New York), an eight-well-array containing eight circular gold-film electrodes with four different diameters, two of which with diameter 50 μm, were used. A 4-kHz ac signal with voltage amplitude 10 mV was applied to the counter electrode and the current (<1 μA) was measured at the working electrode using a current-to-voltage converter made of a TL071CP operational amplifier (Texas Instruments Inc., Dallas, Texas) and a 560 kΩ metal oxide resistor. Amplitudes of analog input-output signals V_{in} and V_{out} from the CSIS were converted and sampled with DAQ hardware at sampling frequency 4 MHz and displayed and stored with LABVIEW software. With the current V_{out}/R and Ohm's law the impedance was calculated as $Z = V_{\text{in}}/I_{\text{out}} = RV_{\text{in}}/V_{\text{out}}$.

MEAs were mounted into a MEA1060UP interface kit (Multi Channel Systems, Reutlingen, Germany), or, alternatively, if eight-well arrays were used, into a custom-made interface. Cells on MEAs were observed with an upright microscope (IX61, Olympus) or an inverted microscope (IX71, Olympus) when eight-well arrays were used. The inverted microscope was equipped with a XM10 (Olympus, Tokyo, Japan) camera. Both types of MEAs were equipped with culture chambers to accommodate cells and culture medium on top of the microelectrodes. Measurements of the complex impedance $Z = |Z|\ \exp(i\,\Delta\phi)$ require the measurement of voltage $|V_{\text{in}}|$, current $|V_{\text{out}}|/R$ and phase shift $\Delta\phi$ of voltage and current caused by the impedance of the sample. In Ref. [28], it was demonstrated that the kinetics of the real part of Z, the resistance, acts most sensitively to cell-substrate or intercellular interactions of an established cell layer at frequencies of 1–10 kHz, whereas the imaginary part, the reactance (respectively capacitance), acts upon the establishment of a cell layer at frequencies >10 kHz, i.e., when cells attach to the electrode-electrolyte interface. Therefore, for single cell-substrate interaction measurements, the phase shift was neglected and the kinetics of the magnitude of Z recorded at 4 kHz (at this frequency, the observed change of $|Z|$ due to cell micromotion was the strongest). The kinetics of impedance and time-lapse bright-field microscopy of selected single *D. discoideum* cells were simultaneously recorded to assess possible correlations between impedance fluctuations and shape changes of the cell.

B. Data processing and analysis

To capture shape changes of a cell, we determined the time evolution of the projected area of a cell on a two-dimensional surface. Images were processed with an edge-detecting algorithm, which finds and fills the closed contour of the cell. We then subtracted the background and performed binary thresholding. Computing the pixel variance of the binary images yielded a white cell surrounded by a black contour line. The contour lines were then closed by further increasing the pixel variance. Finally, the area within the closed-contour objects was filled as shown in Fig. 2(c) and 2(d).

To extract the characteristic periods of shape oscillations of a cell (motility cycle period) from impedance data, we implemented the continuous *wavelet transform* and its time-scale representation, the *scalogram*, in MATLAB, using the Morlet wavelet. A similar approach has been used earlier to analyze oscillatory dynamics during starvation-induced cAMP signaling in *Dictyostelium* [29]. First, each time series of raw impedance data was wavelet transformed. In a second step, its time dependence was removed by element summation of the scale columns in the scalogram. The resulting time-averaged scalograms displayed several characteristic peaks which were assigned to particular persistent scales. The peak corresponding to the lowest oscillation period was selected to determine the motility cycle periods as shown in Fig. 3(d).

The magnitude of impedance fluctuations was quantified by calculating the standard deviation of impedance signals after linear trends were removed; see Fig. 3(c).

C. Cell culture and mutant strains

The cell lines used in our experiments were *Dictyostelium discoideum* AX2-WT cells (kindly provided by R. Gräf, University of Potsdam) and the mutant strains *tal*A$^-$ (dictyBase-strain ID DBS0236177), *nap*A$^-$ (dictyBase-strain ID DBS0236597), *amp*A$^-$ (dictyBase-strain ID DBS0235493), which were ordered from the Dictyostelium Stock Center (dictybase.org). The AX2-derived *GFP-α-tubulin* expressing strain was kindly provided by G. Gerisch (MPI of Biochemistry, Martinsried, Germany). Cells were grown from frozen spores by incubation in HL5 medium (Foremedium) for up to 4 days at 20°C. Cells were then transferred into culture flasks containing HL5 medium until a cell density of 2×10^6 cells per ml was reached. Finally, all cell lines were inoculated at 5×10^5 cells per ml in 25 ml HL5 medium and grown on a shaker at 150 revolutions per minute (rpm) and 20°C for about 20 h.

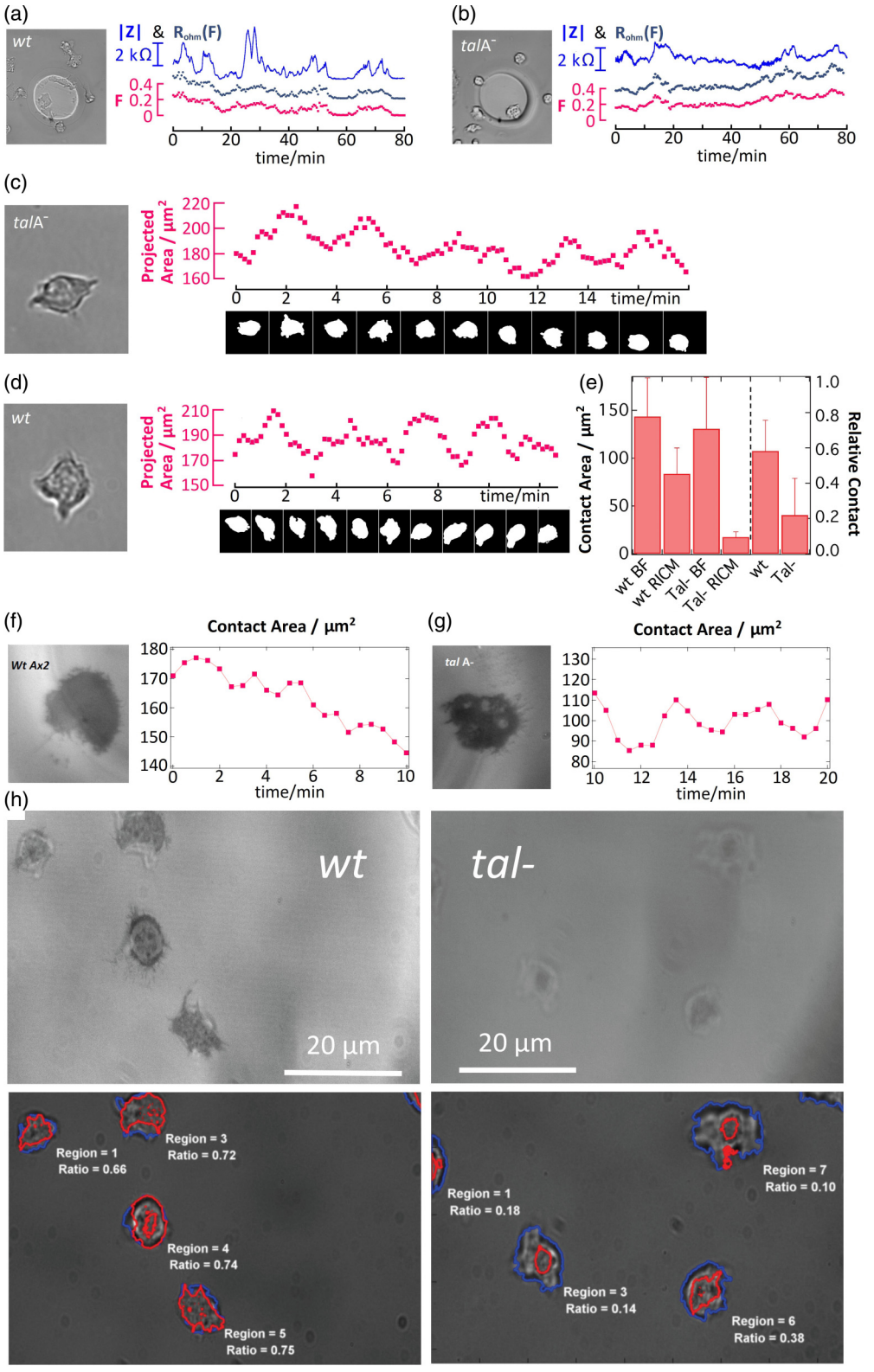

FIG. 2. Time evolution of impedance $|Z|$ (upper line), modeled ohmic resistance $R_{ohm}(F)$ (middle line) and normalized projected area F (bottom line) for (a) AX2-WT and (b) *tal*A$^-$ cells. Time evolution of the projected area for (c) a selected AX2 cell and (d) a *tal*A$^-$ cell, shown together with the corresponding cell shapes. (e) Averaged projected cell area and contact area obtained from bright-field (BF) and reflection interference contrast microscopy (RICM) for WT and *tal*A$^-$ cells and the corresponding ratios (relative contract). (f, g) Time evolution of the contact area (RICM) for a WT and a *tal*A$^-$ cell. (h) Examples of BF and RICM images of WT and *tal*A$^-$ cells. Contact area (RICM, red lines) and contour area (BF, blue lines).

D. Detachment assay

Cell-substrate adhesion of wild-type cells and mutant strains was assessed by a detachment assay as described in Refs. [30,31], exposing cells to fluid shear stress. An amount of 3 ml of cell suspension at a density of 8×10^5 cells/ml were filled into a six-well plate made of polysterene (Sarstedt AG, Nümbrecht, Germany) and cells were allowed for 10 min to sediment and attach to the bottom of the wells. The final cell density in each of the six wells was 2.5×10^5 cells/cm^2. The plate was shaken at 150 rpm and after 0, 5, 15, 30, 45, and 60 min of shaking the supernatant medium was replaced by fresh HL5 medium. Detached cells in the supernatant medium were counted using a hemocytometer. The percentage of detached cells of a well was calculated by summing up all cells counted up to the indicated time points and dividing the sum by the number of attached cells at time point 0 min. Finally, means and standard deviations of the calculated percentages of the six wells of a plate were taken. Results are shown in Fig. 3(f).

E. Single-cell force spectroscopy

As a further method to assess the substrate adhesion strength of single cells, we used an AFM-based single-cell force spectroscopy (SCFS) (Asylum MFP-3D, Asylum Research Wiesbaden, Germany) setup with a 30-μm z range. We functionalized a tipless cantilever (Arrow TL2, NanoWorld, $f_o = 6$ kHz, $k = 0.03$ N/m) with CellTak® (1:30 diluted with 1 mM $NaCO_3$) and immobilized a single cell at the front of the cantilever by picking. After a regeneration time of 2 min, we pressed (trace) the cell with a velocity of 2.5 μm/s and a force of 0.5 nN against an untreated, ethanol-cleaned glass surface for 30 s followed by the detachment (retrace). We repeated this cycle up to 20 times, with a regeneration time of 30 s between each cycle. Cells were measured in the interval from 0 to 3 h after exchange of medium to phosphate buffer. As a result, a characteristic force-distance curve was obtained, from which the maximal adhesion force $F_{\max}$ could be extracted. Results are shown as boxplots in Fig. 3(e).

III. RESULTS

In this section, we present impedance time series of single amoeboid cells on microelectrodes. In the absence of cells, the current flow between working and counter electrodes is only restricted by the bulk electrolyte resistance. Cells partly covering the working electrode surface cause a measurable increase of the impedance due to their insulating membranes; i.e., the coverage of the electrode surface reduces the area available for current flow. While motile *Dictyostelium* amoebae spread and attach on two-dimensional surfaces, they undergo morphological changes from a small round shape to a large flat shape and vice versa. Protrusion of pseudopods followed by retraction of the cell's tail constitute the basic steps in amoeboid motility. During protrusion, the projected area of the cell increases and during retraction it decreases. We show that such cyclic morphological changes are reflected in similar oscillations of the impedance kinetics. However, we also provide evidence that the observed oscillations and fluctuations in the impedance kinetics do not arise solely from changes of the projected area of a cell. In addition, nanometer variations of the cleft between the cell's ventral side and the electrode surface, possibly related to the formation of adhesion sites, strongly affect the impedance signal.

A. Time evolution of the projected area and the overall trend of impedance data correlate

In Figs. 2(a) and 2(b), impedance measurements of vegetative wild type and *tal*A$^-$ cells are shown. All measurements were carried out on identical gold-film electrodes (diameter 50 μm, Applied Biophysics, Troy, New York) under identical conditions. During measurement, the cells were imaged using an inverted microscope to capture variations of the projected cell area. Between one and three cells were located on the electrode surface while the impedance was recorded for 80 min [upper line in Figs. 2(a) and 2(b)]. The projected cell area was calculated as described in the methods section. Quantity F shows the ratio of the projected area and the electrode surface area [bottom line in Figs. 2(a) and 2(b)]. Comparison of impedance data and corresponding F values reveals that the slow irregular oscillations of $|Z|$ resemble those of F (on a timescale of several minutes); i.e., F appears as the underlying trend in the time evolution of the impedance. To quantify this observation, we computed correlation coefficients $C = \mathrm{Cov}(|Z|, F)/\sigma_{|Z|}\sigma_F$, where Cov(.,.) is the covariance, σ is the standard deviation, and thus $C \in [-1,1]$. For the data of AX2-WT and *tal*A$^-$ mutants given in Figs. 2(a) and 2(b) the computed correlation coefficients were $C(\mathrm{WT}) = 0.66$ and $C(tal\mathrm{A}^-) = 0.43$. Thus, both data sets show positive correlation in the time course of impedance and normalized projected area.

To reveal the dependence of the impedance on the projected cell area, we used a classical electrostationary model introduced in Ref. [32] to calculate the ohmic potential in the vicinity of a small disk electrode. In this model, the interaction of a cell with its substrate, notably the formation of sites of close contact, is not explicitly taken into account. Thus the corresponding parameter, the cell-substrate distance h, can be considered constant in this model. The total ohmic resistance can be calculated from Ohm's law and depends inversely on the electrode radius. Considering a cell located on top of the electrode, it can easily be shown that the ohmic resistance depends approximately linearly on the projected cell area. As shown in Figs. 2(a) and 2(b), time courses of modeled ohmic resistance $R_{\mathrm{ohm}}(\mathrm{F})$ and normalized projected area F are proportional, so there is a positive correlation between the measured impedance $|Z|$ and $R_{\mathrm{ohm}}(\mathrm{F})$. Based on this observation, we conjecture that long-term oscillatory trends in the impedance data are mainly related to changes in the projected cell area.

B. A cell line that is deficient in cell-substrate adhesion shows reduced impedance fluctuations

We also observed in the data shown in Figs. 2(a) and 2(b) that AX2-WT cells produced fluctuations in $|Z|$ that are higher in magnitude than those of *tal*A$^-$ cells—a mutant that is known to be strongly defective in substrate adhesion [7]. We quantified

this observation by computing standard deviations of AX2-WT and *tal*A$^-$ impedance time series from Figs. 2(a) and 2(b). Before taking the standard deviations, the lowest oscillatory trend was removed from data by subtracting a polynomial fit of second order. We found that fluctuations in the time series of impedance measured for AX2-WT were about twice as large as those of *tal*A$^-$ cells; $\sigma(\mathrm{WT}) = 826\ \Omega$ and $\sigma(tal\mathrm{A}^-) = 447\ \Omega$. The projected area of AX2-WT cells is smaller or equal to that of *tal*A$^-$ cells in Figs. 2(c) and 2(d). Therefore, changes in the size of the projected cell area cannot be the cause of larger impedance fluctuations.

In Fig. 2(e), we show a comparison of the cell-substrate contact area, viewed in reflection interference contrast microscopy (RICM), and the projected cell area, viewed in bright-field microscopy, of AX2-WT and *tal*A$^-$ cells. In agreement with Ref. [7], we find that in the less adhesive *tal*A$^-$ cells, the substrate contact area is strongly reduced. Examples of the contact area and the projected cell area for both cell lines are shown in Fig. 2(h). The time evolution of the substrate contact area of an AX2-WT and a *tal*A$^-$ cell determined from RICM images can be seen in Figs. 2(f) and 2(g). These time traces display a slow oscillatory trend, similar to the time evolution of the projected area in Figs. 2(a) and 2(b). We thus conclude that rapid fluctuations in the impedance amplitude are related neither to the projected cell area nor to the contact area as imaged by RICM. They rather arise from the formation of local adhesion sites leading to changes in the cell-substrate distance within the contact area.

C. Standard deviations of detrended impedance time series correspond to the cell-substrate adhesion strengths

To systematically explore the relation between cell-substrate adhesion and fluctuations in the impedance signal, we have collected more than a hundred single-cell impedance time series from AX2-WT cells and the four mutant strains *tal*A$^-$, *nap*A$^-$, *amp*A$^-$, and *GFP-α-tubulin* with different adhesion properties. We used MEAs with 59 square electrodes ($50 \times 50\ \mu\mathrm{m}^2$) arranged on a square grid, with equal distances of 200 μm between them. If vegetative cells at low density were seeded into the culture chamber, some electrodes were found with just a single cell on top. In each experiment, four such electrodes were selected and simultaneously recorded. In this way, at least 20 single-cell impedance time series of approximately 30 min were recorded for every cell line (20 time series for WT, *nap*A$^-$, and *amp*A$^-$; 26 for *tal*A$^-$; and 32 for *GFP-α-tubulin*).

In Fig. 3(a), five selected examples of our single-cell measurements are displayed. The impedance signals show typical irregular oscillations arising from correlated shape changes of single cells attached to the electrode. We applied the wavelet transform to the impedance time series to find the characteristic scale representing the motility cycle period as described in Sec. II. The interesting range, where characteristic scales occurred, was 1–800 (the relation between scale a of the Morlet wavelet and the period p is given by $p = ca$ with $c \approx 1.23$). In our data, three scales in the relevant range were identified in the scalograms for the predominant part of all time series. The scales change over time due to nonstationarities and alterations of the motility cycle period of a cell. To identify the dominant scales of a time series, the wavelet coefficients $|X_W(a,b)|^2$ were time averaged. The averaged wavelet transforms are shown to the right of each scalogram in Fig. 3(b). The characteristic scales correspond to the local maxima in the averaged scalograms. For different time series, the maxima may occur at different positions and with different weights.

The smallest persistent scale in an averaged scalogram represents the smallest characteristic oscillation period of the signal. We used this scale (i.e., the corresponding period) as the characteristic motility cycle period of a given cell. This scale was marked by a red vertical line in Fig. 3(b). The averaged motility cycle periods are shown in Fig. 3(d). Above the averaged scalograms of Fig. 3(b), the corresponding power spectra are shown. Obviously, in most cases, the same three-scale structures as in the scalograms appear. But only from the scalograms can it be easily reconstructed how scales evolve over time.

After removing linear trends, the standard deviations of fluctuations of impedance signals were computed to quantify their amplitudes. Results are presented as boxplots in Fig. 3(c). We observed a correlation between the standard deviations of the detrended impedance time series and the adhesion strengths measured independently by the fraction of detached cells in the shear stress detachment assay respectively cantilever picking of single cells by AFM-SCFS (see Sec. II for a detailed description of independent adhesion measurements). The largest standard deviations are found for the strongly adhesive cell lines *GFP-α-tubulin*, AX2-WT, and *amp*A$^-$ (impedance analysis and cantilever picking reveal *amp*A$^-$ as the most strongly adhesive cell line, while in the shear stress detachment analysis *GFP-α-tubulin* is the strongest). All methods clearly reveal *tal*A$^-$ and *nap*A$^-$ as the cells with the weakest adhesion strength.

No such trend is found for the motility cycle periods derived from impedance data [Fig. 3(d)]. Cycle periods of *tal*A$^-$ cells do not deviate significantly from those of other cells. Similarly, the motility cycle periods derived from projected cell area data for AX2-WT and *tal*A$^-$ cells [see Figs. 2(c) and 2(d), and Figs. 4 and 5 in the Appendix] do not significantly differ from those calculated from impedance data.

IV. DISCUSSION

In this experimental study, single cells of *Dictyostelium discoideum* AX2 wild type and four mutant strains, *tal*A$^-$, *nap*A$^-$, *amp*A$^-$, and *GFP-α-tubulin*, were measured using a custom designed cell-substrate impedance sensor, which allowed for simultaneous recording of impedance data and for video microscopy.

A. Influence of mutations on cell-substrate adhesion

We chose *D. discoideum* mutant strains according to their different cell-substrate adhesiveness compared to AX2-WT cells. Talin is one of the actin binding proteins which anchors filamentous actin to the plasma membrane. Phenotypic alterations of *tal*A$^-$ cells include larger cell sizes, a more "blebbing"-like shape than wild type, and weaker adhesion

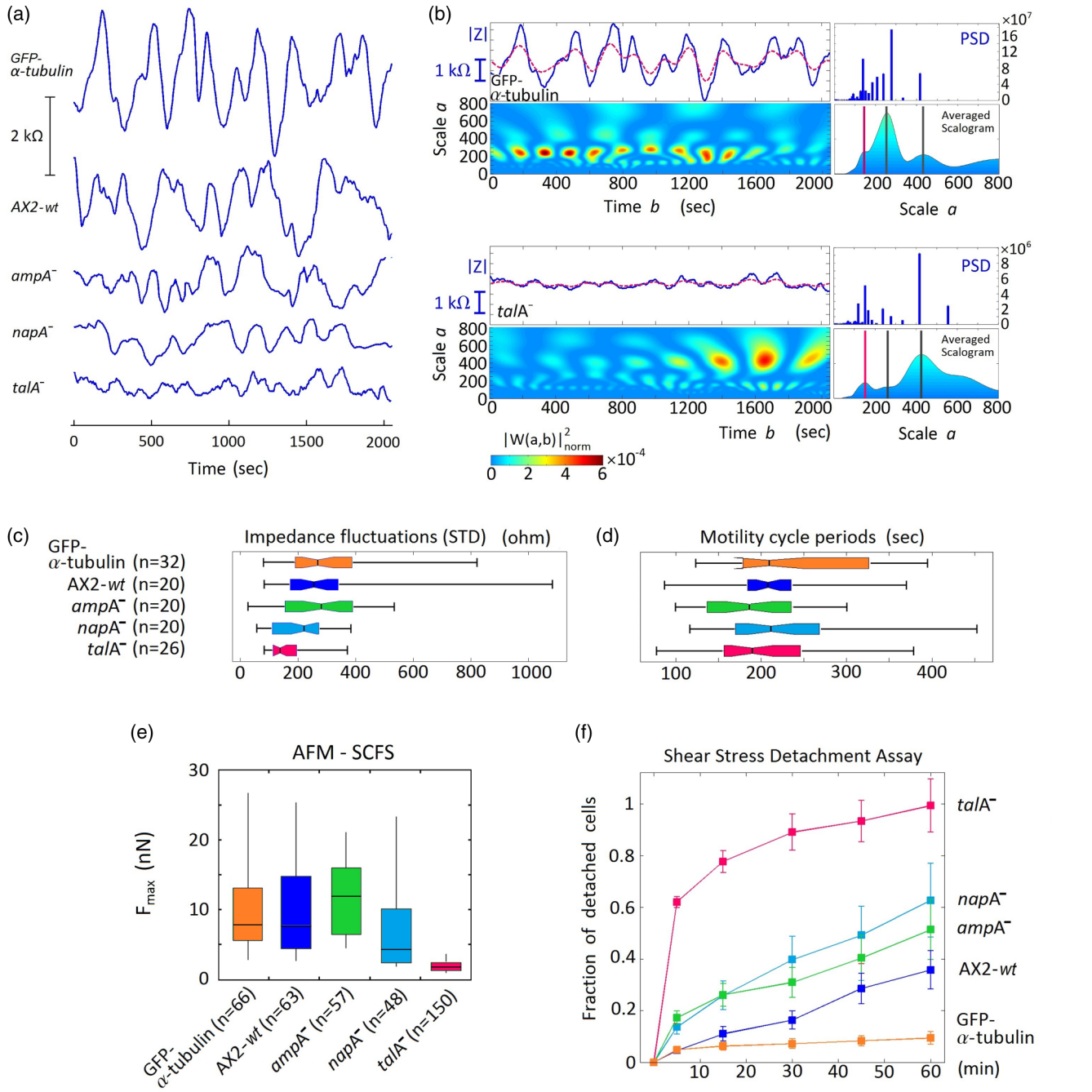

FIG. 3. (a) Selected impedance time series for every cell line. (b) Wavelet scalograms for *GFP-α-tubulin* and *tal*A$^-$ impedance time series. Low-pass filtered signals (dashed lines). On the right-hand side time-averaged scalograms and power spectra (PSD) are shown. (c) Standard deviations of high-pass filtered impedance signals. (d) Motility cycle periods. (e) Maximal adhesion force measured with AFM-SCFS. (f) Shear stress detachment assay. At indicated time points detached cells were counted.

to surfaces [7]. The protein *nap*A was shown to be involved in regulation of actin nucleation. Knockout mutants of *nap*A, made by homologous recombination in wild-type strain AX3, have a smaller and more rounded shape than the wild type, chemotax slower, protrude smaller pseudopods, and have defects in cell-substrate adhesions [33]. The protein *amp*A (adhesion modulation protein A) plays a role in cell migration and adhesion during development. For *amp*A knockout mutants an increased substrate adhesion was reported. The vegetative *amp*A null cells were largely unable to migrate toward folic acid and they protrude fewer and more rounded pseudopods. Consistently, *amp*A$^-$ cells polymerize less actin while overexpressing cells polymerize more actin than wild type [34]. In our detachment assay, *amp*A$^-$ showed a weaker substrate adhesion strength than the wild type, in contrast to the magnitude of impedance fluctuations and the maximal adhesion force measured by cantilever picking, which assessed *amp*A$^-$ cells as stronger adhesive than wild type.

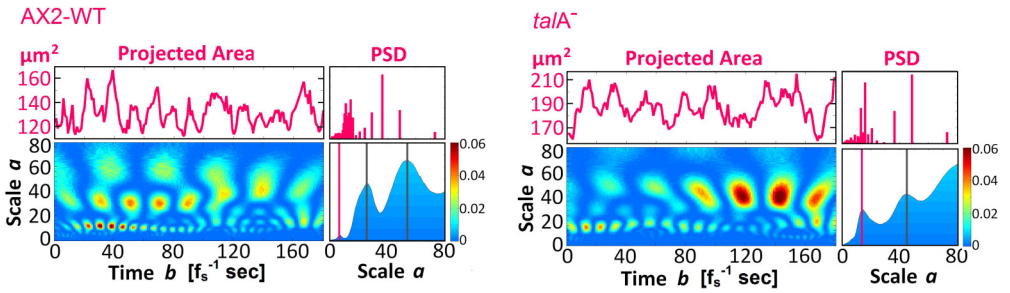

FIG. 4. Selected time series of the projected area, wavelet scalogram, time-averaged scalogram, and power spectrum for an AX2 cell and a *tal*A⁻ cell.

B. Impedance time series encode cell shape and adhesion dynamics

Surface-attached single motile amoeboid cells undergo oscillatory shape changes. Alternating protrusion and retraction constitute a motility cycle, which appears as the basic pattern of all forms of movement and taxis over various substrata [35]. This process is associated with the formation of adhesion sites. Thus, the motility of amoebae can be seen as a combination of (1) *shape oscillations* due to periodic increase (protrusions) and decrease (retractions) of the projected cell area and (2) *cell-substrate interactions*, comprising the formation of traction stress patterns, adhesion regions, and possibly other events taking place in the cell-substratum gap.

In our experiments, all impedance time series of single vegetative amoebae are characterized by irregular oscillations. Successive minima of oscillations correspond to a compact cell shape as the start and end point of a motility cycle. An impedance model reveals that indeed the projected cell area is encoded in these long-term trends of the impedance kinetics. Characteristic scales of the motility cycles and their alteration over time were uncovered by computing wavelet scalograms, as described in Secs. II and III. The most persistent scales were obtained by time-averaging the scalograms.

Superposed to these oscillatory long-term trends, we observed fluctuations in the impedance signal. In order to quantify the impedance fluctuations, we subtracted a linear fit from our data and computed standard deviations of the resulting signals [Fig. 3(c)] as a measure of the amplitude of fluctuations. By comparison with two independent adhesion assays, we found that the amplitude of impedance fluctuations correlates with the adhesion strength. Taken together, all methods shown in Fig. 3 reveal *GFP-α-tubulin*, AX2-WT, and *amp*A⁻ as the strongest adhesive cell lines. Within this group, impedance fluctuations and the maximal adhesion force [Fig. 3(e)] assess *amp*A⁻ as the strongest adhesive cell line. In the shear stress detachment assay, this is the case for *GFP-α-tubulin* cells. All methods produced consistent results regarding the group of cell lines with weak adhesion strength, *nap*A⁻ and *tal*A⁻.

We conjecture that the fluctuations are associated with the formation of localized cell-substrate adhesion sites. The correlation of fluctuation magnitude and adhesion strength suggests that cells with more dynamic cell-substrate interactions are less prone to detachment. Reflection interference contrast microscopy confirms that adhesion relies on regions of close contact between the ventral cell membrane and the substrate and does not depend on the projected cell area. However, the fluctuating dynamics of individual adhesion sites within these contact regions cannot be resolved with this method.

In contrast to the correlation between fluctuations and adhesion strength, differences between the motility cycle periods of the different cell lines are not statistically significant [see Figs. 3(d) and 5]. This suggests that the adhesion strength of a cell does not affect its motility cycle period (except in the cases of very weak or strong adhesion). A possible interpretation of this observation is that soil-living *Dictyostelium* amoebae have to cope with a variety of substrates of different adhesiveness, where maintenance of a robust motility cycle is an important function for survival under these conditions. In future work, we will focus on the relation between fluctuations in the impedance signal and periodic dynamics in the actin cytoskeleton [36]. Also the relation to random components in the cell trajectories will be explored [37–39].

ACKNOWLEDGMENTS

We thank Christian Westendorf and Hannes Witt for help and assistance. We acknowledge financial support of the Ministerium für Wissenschaft, Forschung und Kultur des Landes Brandenburg together with the Europäischer Fond für regionale Entwicklung (EFRE) (Grants No. 80147097, No. 80148364, and No. F111-02-UNIP/003 to C.B.) and by the Deutsche Forschungsgemeinschaft (Grant No. BE 3978/3-1 to C.B. and SFB 937 project A8 to M.T. and project A9 to C.B.).

APPENDIX: MEASUREMENTS OF PROJECTED CELL AREA

The time course of the projected cell area for AX2-WT and *tal*A⁻ cells was independently recorded from impedance measurements to test whether irregular impedance oscillations arise from those of the projected area. Images from time-lapse microscopy were processed as described in the Method section and 25 time series of length >1 h were recorded for

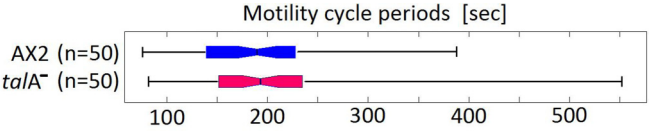

FIG. 5. Motility cycle periods calculated from projected cell area time series.

WT as well as *tal*A$^-$ cells, giving 50 short time series of 0.5 h for both cell lines. Characteristic scales were found with the same wavelet-based analysis as for impedance time series (Fig. 4).

To compare scales of the projected area with those of the impedance, note that the sample frequencies were different for both data sets (for impedance data and for projected area data); i.e., the scales of the projected area must be multiplied with the corresponding sample period of approximately 10 s to make them comparable to the scales of the impedance. Figure 5 shows computed motility cycle periods (corresponding to the smallest persistent scale found in the averaged scalograms). No significant difference can be found between cycle periods of WT and *tal*A$^-$ cells. The same also holds if the cycle periods are compared to those derived from impedance data [Fig. 3(d)].

[1] R. Zaidel-Bar, S. Itzkovitz, A. Ma'ayan, R. Iyengar, and B. Geiger, Nat. Cell Biol. **9**, 858 (2007).

[2] J. D. Humphries, A. Byron, and M. J. Humphries, J. Cell Sci. **119**, 3901 (2006).

[3] I. Kaverina, O. Krylyshkina, and J. V. Small, Int. J. Biochem. Cell Biol. **34**, 746 (2002).

[4] B. Geiger, J. P. Spatz, and A. D. Bershadsky, Nat. Rev. Mol. Cell Biol. **10**, 21 (2009).

[5] H. Wolfensohn, Y. I. Henis, B. Geiger, and A. D. Bershadsky, Cell Mot. Cytoskel. **66**, 1017 (2009).

[6] I. Weber, E. Wallraff, R. Albrecht, and G. Gerisch, J. Cell Sci. **108**, 1519 (1995).

[7] J. Niewöhner, I. Weber, M. Maniak, A. Müller-Taubenberger, and G. Gerisch, J. Cell Biol. **138**, 349 (1997).

[8] S. Cornillon, E. Pech, M. Benghezal, K. Ravanel, E. Gaynor, F. Letourneur, F. Brückert, and P. Cosson, J. Biol. Chem. **275**, 34287 (2000).

[9] P. Fey, S. Stephens, M. A. Titus, and R. L. Chisholm, J. Cell Biol. **159**, 1109 (2002).

[10] T. R. Varney, E. Casademunt, H. N. Ho, C. Petty, J. Dolman, and D. D. Blumberg, Dev. Biol. (Amsterdam, Neth.) **243**, 226 (2002).

[11] S. Cornillon, L. Gebbie, M. Benghezal, P. Nair, S. Keller, B. Wehrle-Haller, S. J. Charette, F. Brückert, F. Letourneur, and P. Cosson, EMBO Rep. **7**, 617 (2006).

[12] W. F. Loomis, D. Fuller, E. Gutierrez, A. Groisman, and W.-J. Rappel, PLoS One **7**, e42033 (2012).

[13] M. Tarantola, A. Bae, D. Fuller, E. Bodenschatz, W.-J. Rappel, and W. F. Loomis, PLoS One **9**, e106574 (2014).

[14] K. S. K. Uchida and S. Yumura, J. Cell Sci. **117**, 1443 (2004).

[15] B. Alvarez-Gonzalez, R. Meili, E. Bastounis, R. A. Firtel, J. C. Lasheras, and J. C. del Alamo, Biophys. J. **108**, 821 (2015).

[16] J. C. del Alamo, R. Meili, B. Alonso-Latorre, J. Rodriguez-Rodriguez, A. Aliseda, R. A. Firtel, and J. C. Lasheras, Proc. Natl. Acad. Sci. U.S.A. **104**, 13343 (2007).

[17] R. Meili, B. Alonso-Latorre, J. C. del Alamo, R. A. Firtel, and J. C. Lasheras, Mol. Biol. Cell **21**, 405 (2010).

[18] M. Sabouri-Ghomi, Yi Wu, K. Hahn, and G. Danuser, Curr. Opin. Cell Biol. **20**, 541 (2008).

[19] V. Perumal and U. Hashim, J. Appl. Biomed. **12**, 1 (2014).

[20] I. Giaever and C. R. Keese, Proc. Natl. Acad. Sci. U.S.A. **81**, 3761 (1984).

[21] I. Giaever and C. R. Keese, Proc. Natl. Acad. Sci. U.S.A. **88**, 7896 (1991).

[22] L. di Blasio, P. A. Gagliardi, A. Puliafito, R. Sessa, G. Seano, F. Bussolino, and L. Primo, J. Cell Sci. **128**, 863 (2015).

[23] N. Ke, X. Wang, X. Xu, and J. A. Abassi, Methods Mol. Biol. **740**, 33 (2011).

[24] P. A. Gagliardi, A. Puliafito, L. di Blasio, F. Chianale, D. Somale, G. Seano, F. Bussolino, and L. Primo, Sci. Rep. **5**, 10206 (2015).

[25] K. M. Pietrosimone, X. Yin, D. A. Knecht, and M. A. Lynes, J. Visualized Exp. **62**, e3840 (2012).

[26] E. Schäfer, C. Westendorf, E. Bodenschatz, C. Beta, B. Geil, and A. Janshoff, Small **7**, 723 (2011).

[27] E. Schäfer, M. Tarantola, E. Polo, C. Westendorf, N. Oikawa, E. Bodenschatz, B. Geil, and A. Janshoff, PLoS One **8**, e54172 (2013).

[28] J. Wegener, C. R. Keese, and I. Giaever, Exp. Cell Res. **259**, 158 (2000).

[29] S. Sawai, P. A. Thomason, and E. C. Cox, Nature (London) **433**, 323 (2005).

[30] L. Bosgraaf, A. Waijer, R. Engel, A. J. G. W. Visser, D. Wessels, D. Soll, and P. J. M. van Haastert, J. Cell Sci. **118**, 1899 (2005).

[31] E. K. B. Pfannes, M. Theves, C. Wegner, and C. Beta, J. Muscle Res. Cell Motil. **33**, 95 (2012).

[32] Yu. V. Pleskov and V. Yu. Filinovskii, *The Rotating Disk Electrode* (Springer, Berlin, 2012).

[33] N. Ibarra, S. L. Blagg, F. Vazquez, and R. H. Insall, Curr. Biol. **16**, 717 (2006).

[34] E. F. Noratel, C. L. Petty, J. S. Kelsey, H. N. Cost, N. Basappa, and D. D. Blumberg, BMC Cell Biol. **13**, 29 (2012).

[35] P. J. M. Van Haastert and A. N. Hotchin, PLoS One **6**, e27532 (2011).

[36] C. Westendorf, J. Negrete, Jr., A. J. Bae, R. Sandmann, E. Bodenschatz, and C. Beta, Proc. Natl. Acad. Sci. U.S.A. **110**, 3853 (2013).

[37] G. Amselen, M. Theves, A. Bae, E. Bodenschatz, and C. Beta, PLoS One **7**, e37213 (2012).

[38] H. U. Bödeker, C. Beta, T. D. Frank, and E. Bodenschatz, Europhys. Lett. **90**, 28005 (2010).

[39] N. Makarava, S. Menz, M. Theves, W. Huisinga, C. Beta, and M. Holschneider, Phys. Rev. E **90**, 042703 (2014).